Chapter 5

CONSTRAINED TRANSPORT

In this chapter we consider a technique that can be coupled with the wave propagation method for keeping the magnetic field divergence-free in the ideal MHD and SMHD equations. We begin by explaining why it is necessary to exactly eliminate magnetic monopoles. We then review three Godunov-type methods from the literature, each with the property that the divergence of the magnetic field is identically zero for all space and time. Finally, we describe why it it necessary to improve these methods and we propose a novel approach based on TVD ideas.

5.1 The divergence-free constraint

Magnetic monopoles have never been found either in nature or in the laboratory. In Maxwell's equations this fact translates into the following constraint on the magnetic field:

$$\nabla \cdot \mathbf{B} = 0\,. \tag{5.1}$$

If the initial magnetic field obeys this divergence-free constraint, Faraday's law guarantees that it remains divergence-free for all time:

$$\begin{aligned} & \partial_t \mathbf{B} + \nabla \times (\mathbf{B} \times \mathbf{u}) = 0 \\ \Longrightarrow \quad & \nabla \cdot \partial_t \mathbf{B} + \nabla \cdot \nabla \times (\mathbf{B} \times \mathbf{u}) = 0 \\ \Longrightarrow \quad & \partial_t \left(\nabla \cdot \mathbf{B} \right) = 0. \end{aligned}$$

Although $\nabla \cdot \mathbf{B} = 0$ is guaranteed in the continuous MHD equations, many numerical discretizations can only guarantee that the divergence is of the order of the truncation error:

$$\nabla \cdot \mathbf{B} = \mathcal{O}(\Delta x^p, \Delta y^p). \tag{5.2}$$

Near shock waves or other discontinuities the divergence may become very large:

$$\nabla \cdot \mathbf{B} \gg 1\,. \tag{5.3}$$

Furthermore, recall that the divergence wave in both ideal MHD and SMHD is always stationary (see Chapters 3 and 4). This implies that the divergence errors are permanent in space; and therefore, they have the ability to grow in a localized region in space over time.

Recall from Chapter 3 that the Lorentz force is given by

$$F_\ell = (\mathbf{J} \times \mathbf{B})\,. \tag{5.4}$$

The divergence-free constraint tells us that the component of the Lorentz force along the magnetic field should always vanish:

$$F_\ell \cdot \mathbf{B} = (\mathbf{J} \times \mathbf{B}) \cdot \mathbf{B} = |\mathbf{B}|^2 \left(\nabla \cdot \mathbf{B} \right) = 0. \tag{5.5}$$

In a paper published in 1980, Brackbill and Barnes [12] show that the build up of divergence error generates a spurious Lorentz force along the magnetic field. This error leads to the possible production of negative pressure and density in the case of ideal MHD and negative height in the case of SMHD. It has been shown repeatedly in the literature that special treatment must be given to the magnetic field in order to avoid spurious solutions (see Tóth [90] for a review).

5.2 *A review of available methods for magnetohydrodynamics*

In this section we briefly review four methods for solving the magnetohydrodynamic equations. For simplicity we formulate all of the methods below for the SMHD equations. In all cases the generalization to ideal MHD is straightforward.

5.2.1 The projection method

The projection method is conceptually the easiest and probably most widely used method for solving the MHD equations. This is the method advocated in Brackbill and Barnes [12] and Tóth [90]. The idea is to *predict* the value of the magnetic field through some cell centered finite volume method and then *correct* this value by projecting it to its divergence-free subspace. A single step of a finite volume method yields

$$\left[h^n,\ u_1^n,\ u_2^n,\ \mathfrak{B}_1^n,\ \mathfrak{B}_2^n\right] \Longrightarrow \left[h^{n+1},\ u_1^{n+1},\ u_2^{n+1},\ \mathfrak{B}_1^\star,\ \mathfrak{B}_2^\star\right]. \tag{5.6}$$

We can decompose the predicted magnetic field in the following way:

$$\boldsymbol{\mathfrak{B}}^\star = \nabla \times \mathbb{A} + \nabla\phi\,. \tag{5.7}$$

Taking the divergence of both sides yields

$$\nabla^2\phi = \nabla\cdot\boldsymbol{\mathfrak{B}}^\star\,. \tag{5.8}$$

If this Poisson equation for the potential ϕ is solved, then the divergence-free magnetic field at time $t = t_{n+1}$ is given by

$$\boldsymbol{\mathfrak{B}}^{n+1} = \boldsymbol{\mathfrak{B}}^\star - \nabla\phi\,. \tag{5.9}$$

The standard approach is to approximate $\nabla\phi$ and $\nabla^2\phi$ by the following finite difference operators in order to make $\nabla\phi$ a cell centered quantity:

$$[\nabla\phi]_{ij} \approx \left(\frac{\phi_{i+1,j}-\phi_{i-1,j}}{2\Delta x},\ \frac{\phi_{i,j+1}-\phi_{i,j-1}}{2\Delta y}\right) \tag{5.10}$$

$$\left[\nabla^2\phi\right]_{ij} \approx \frac{\phi_{i+2,j}-2\phi_{ij}+\phi_{i-2,j}}{4\Delta x^2} + \frac{\phi_{i,j+2}-2\phi_{ij}+\phi_{i,j-2}}{4\Delta y^2}\,. \tag{5.11}$$

This approach guarantees that the following discrete divergence is identically zero:

$$[\nabla\cdot\boldsymbol{\mathfrak{B}}]_{ij}^n \approx \frac{[\mathfrak{B}_1]_{i+1,j}-[\mathfrak{B}_1]_{i-1,j}}{2\Delta x} + \frac{[\mathfrak{B}_2]_{i,j+1}-[\mathfrak{B}_2]_{i,j-1}}{2\Delta y} = 0\,. \tag{5.12}$$

The main drawback of this method is that by adding to a hyperbolic system of equations an additional elliptic equation, the overall cost of the algorithm is much higher. Furthermore, this approach may introduce some slight oscillations near strong shocks since the elliptic equation is solved to second order.

5.2.2 The 8-wave formulation

In a 1994 paper, Powell [71] introduced the idea of deriving the MHD equations with the assumption that $\nabla \cdot \mathbf{B} \neq 0$. The SMHD analogy (see De Sterck [83]) can be written as

$$\partial_t \begin{bmatrix} h \\ h\mathbf{u} \\ h\mathbf{B} \end{bmatrix} + \nabla \cdot \begin{bmatrix} h\mathbf{u} \\ h\mathbf{u} \otimes \mathbf{u} - h\mathbf{B} \otimes \mathbf{B} + \frac{1}{2} g h^2 \mathcal{I} \\ h\mathbf{u} \otimes \mathbf{B} - h\mathbf{B} \otimes \mathbf{u} \end{bmatrix} = - \begin{bmatrix} 0 \\ \mathbf{B} \\ \mathbf{u} \end{bmatrix} \nabla \cdot (h\mathbf{B}) \, . \tag{5.13}$$

Powell's modification thus introduces an additional source term. Instead of

$$\partial_t \left(\nabla \cdot \mathfrak{B} \right) = 0, \tag{5.14}$$

the time evolution of the divergence is now given by

$$\partial_t \left(\nabla \cdot \mathfrak{B} \right) + \nabla \cdot \left[\mathbf{u} \left(\nabla \cdot \mathfrak{B} \right) \right] = 0 \, . \tag{5.15}$$

This means that any non-zero divergence is no longer stationary; and instead, the divergence error is now advected by the flow. The advantage of this approach is that it is inexpensive compared to the projection method; and furthermore, for problems with outflow boundary conditions, it allows the divergence error to be swept out of the computational domain.

The main disadvantage of this approach is that for problems with periodic or solid wall boundaries the divergence error will still remain inside the computational domain. Furthermore, because we are solving the "wrong" equations, the 8-wave formulation may introduce incorrect jump conditions across strong shocks (see Tóth [90]).

5.2.3 The generalized divergence cleaning method

A generalization of both the projection method and the 8-wave formulation is the divergence cleaning method of Dedner, Kemm, Kröner, Munz, Schnitzer, and Wesenberg [21]. This approach introduces an additional equation into the MHD or SMHD system which governs the error made in the divergence of the magnetic field. This error equation can be made either hyperbolic, parabolic, or elliptic. The approach suggested in [21] is to make the error equation an advection-diffusion equation so that the divergence error is both advected and diffused. The main disadvantage of this approach is that we are solving the "wrong" equations. Again, this can result in incorrect jump conditions across sufficiently strong shocks.

5.2.4 The constrained transport method

The final approach which we consider is the constrained transport method originally considered by Evans and Hawley [22]. The idea in this approach is to stagger the magnetic field in such a way that the divergence of the magnetic field is exactly zero. This method does not require the introduction of modified or additional equations. In particular, we will consider in this work a constrained transport approach that is compatible with the previously described wave propagation method (see Chapter 2). Several variants of the constrained transport method have been considered in the literature [7, 20, 63, 78, 84]. We will not in this work directly consider the methods of Londrillo and Del Zanna [63] and De Sterck [84]. The method of Londrillo and Del Zanna [63] is specific to an ENO (essentially non-oscillatory) scheme based on flux vector splitting and is not directly compatible with the propagation method. The method of De Sterck [84] is based on a finite volume method on a triangular grid and is also not compatible with the wave propagation method.

5.3 Constrained transport on Cartesian grids

In order to keep the discussion open to both MHD and SMHD, it becomes convenient to define the quantity

$$\boldsymbol{\mathfrak{B}} \equiv \begin{cases} \mathbf{B} & \text{if solving 2D ideal MHD} \\ h\mathbf{B} & \text{if solving SMHD}\,. \end{cases} \tag{5.16}$$

The divergence-free constraint for either system can then be written as

$$\nabla \cdot \boldsymbol{\mathfrak{B}} = \partial_x \mathfrak{B}_1 + \partial_y \mathfrak{B}_2 = 0\,. \tag{5.17}$$

We simply refer to $\boldsymbol{\mathfrak{B}} = (\mathfrak{B}_1, \mathfrak{B}_2)^t$ as the magnetic field. Strictly speaking, however, in SMHD this is the depth averaged magnetic field multiplied by the depth of the fluid. Because the magnetic field is divergence-free, we define a *magnetic potential* $\mathbb{A}$ such that

$$\boldsymbol{\mathfrak{B}} = \nabla_3 \times \mathbb{A}\,. \tag{5.18}$$

The magnetic field obeys the *induction equation* discussed in Chapter 3,

$$\partial_t \boldsymbol{\mathfrak{B}} + \nabla_3 \times \begin{bmatrix} 0 \\ 0 \\ \Omega \end{bmatrix} = 0\,. \tag{5.19}$$

Re-writing the induction equation in terms of the previously defined potential yields

$$\partial_t \mathbb{A} + \Omega = 0 \tag{5.20}$$

$$\mathfrak{B}_1 = \partial_y \mathbb{A} \tag{5.21}$$

$$\mathfrak{B}_2 = -\partial_x \mathbb{A}\,. \tag{5.22}$$

By *Ohm's law* for a perfect conductor, the electric field is given by

$$\Omega = \left(-\boldsymbol{u} \times \boldsymbol{\mathfrak{B}}\right) \cdot \hat{\mathbf{k}} = -u_1 \mathfrak{B}_2 + u_2 \mathfrak{B}_1\,. \tag{5.23}$$

In the next section we devise a way to solve (5.20)-(5.22) in a such a way as to keep the magnetic field numerically divergence-free.

5.3.1 The induction equation

Let us momentarily assume that the electric field Ω is known and our goal is to numerically solve for the magnetic field in such a way that a sensible discrete version of (5.17) is exactly satisfied at each time step in the update. As discussed in Tóth [90], a common way to approach this problem is to stagger the numerical grid so that the 1-component of the magnetic field lives on the left and right grid interfaces ($\mathfrak{b}_1$), the 2-component on the top and bottom grid interfaces ($\mathfrak{b}_2$), and the magnetic potential on the grid corners ($\mathbb{A}$). This staggering is depicted in Figure 5.1. The so-called *constrained transport* (CT) update for the magnetic field then takes the form

$$\mathbb{A}^{n+1}_{i-1/2,j-1/2} = \mathbb{A}^{n}_{i-1/2,j-1/2} - \Delta t\, \Omega^{n+1/2}_{i-1/2,j-1/2} \tag{5.24}$$

$$[\mathfrak{b}_1]^{n+1}_{i-1/2,j} = \frac{1}{\Delta y}\left(\mathbb{A}^{n+1}_{i-1/2,j+1/2} - \mathbb{A}^{n+1}_{i-1/2,j-1/2}\right) \tag{5.25}$$

$$[\mathfrak{b}_2]^{n+1}_{i,j-1/2} = \frac{1}{\Delta x}\left(\mathbb{A}^{n+1}_{i-1/2,j-1/2} - \mathbb{A}^{n+1}_{i+1/2,j-1/2}\right). \tag{5.26}$$

It is easy to verify that this update will numerically conserve the following discrete divergence at each time step:

$$[\nabla\cdot\mathfrak{b}]^{n+1}_{ij} \equiv \frac{[\mathfrak{b}_1]^{n+1}_{i+1/2,j} - [\mathfrak{b}_1]^{n+1}_{i-1/2,j}}{\Delta x} + \frac{[\mathfrak{b}_2]^{n+1}_{i,j+1/2} - [\mathfrak{b}_2]^{n+1}_{i,j-1/2}}{\Delta y}. \tag{5.27}$$

Therefore, the staggered magnetic field satisfies $[\nabla\cdot\mathfrak{b}]^{n+1}_{ij} = 0$ if $[\nabla\cdot\mathfrak{b}]^{n}_{ij} = 0$. This reduces to requiring that the initial condition be divergence-free:

$$[\nabla\cdot\mathfrak{b}]^{0}_{ij} = 0\,. \tag{5.28}$$

5.3.2 Obtaining divergence-free initial conditions:

In order to satisfy (5.28) and to apply procedure (5.24), the initial conditions for the magnetic potential must be known. In many cases, however, the initial conditions will only be given in terms of the magnetic field and it may be difficult to obtain an analytic form for the initial $\mathbb{A}$. In this case, we can compute the magnetic potential by solving a Poisson equation of the form:

$$\begin{aligned}
& \nabla\times\mathfrak{B} = \nabla\times\nabla\times\mathbb{A} = \nabla\left(\nabla\cdot\mathbb{A}\right) - \nabla^2\mathbb{A} && \text{(Vector identity)}\\
\Longrightarrow\quad & \nabla^2\mathbb{A} = -\nabla\times\mathfrak{B} && \text{(applied gauge condition)}\\
\Longrightarrow\quad & \partial_x^2\mathbb{A} + \partial_y^2\mathbb{A} = \partial_y\mathfrak{B}_1 - \partial_x\mathfrak{B}_2. && \text{(2D version)}
\end{aligned}$$

Once the initial magnetic potential has been determined, the initial magnetic field should be redefined as a finite difference of the magnetic potential so that it satisfies (5.28):

$$[\mathfrak{b}_1]^{0}_{i-1/2,j} = \frac{1}{\Delta y}\left(\mathbb{A}^{0}_{i-1/2,j+1/2} - \mathbb{A}^{0}_{i-1/2,j-1/2}\right) \tag{5.29}$$

$$[\mathfrak{b}_2]^{0}_{i,j-1/2} = \frac{1}{\Delta x}\left(\mathbb{A}^{0}_{i-1/2,j-1/2} - \mathbb{A}^{0}_{i+1/2,j-1/2}\right). \tag{5.30}$$

We emphasize here that even in the case where the initial magnetic potential is not known analytically, a Poisson equation for the magnetic potential need only be solved at the initial time. During all subsequent time steps the CT update directly produces a magnetic potential that conserves the numerical divergence-free constraint (5.17).

5.3.3 Application to magnetohydrodynamics

The following question now presents itself: How can the above update for the induction equation be used for the more complicated SMHD or MHD equations? In order to answer this, we outline the constrained transport method in terms of the SMHD equations. We begin by first devising a grid staggering in which we define (see Figure 5.2):

$$\begin{aligned} \text{at Cell Centers:} \quad & h_{ij},\ [u_1]_{ij},\ [u_2]_{ij},\ [\mathfrak{B}_1]_{ij},\ [\mathfrak{B}_2]_{ij} \\ \text{at Cell Corners:} \quad & \mathbb{A}_{i-1/2,j-1/2} \\ \text{at Left/Right Edges:} \quad & [\mathfrak{b}_1]_{i-1/2,j} \\ \text{at Top/Bottom Edges:} \quad & [\mathfrak{b}_2]_{i,j-1/2}\,. \end{aligned}$$

Furthermore, we refer to the grid on which h_{ij} is defined as the primary or $\mathcal{P}$-grid and the grid on which $\mathbb{A}_{i-1/2,j-1/2}$ is defined as the secondary or $\mathcal{S}$-grid (see Figure 5.2). With these definitions, the following algorithm can be used to obtain a update for the SMHD equations that maintains a divergence-free magnetic field (see also the flowchart in Figure 5.3):

Step 0. Primary quantities: $\boxed{h^n,\ u_1^n,\ u_2^n,\ \mathfrak{b}_1^n,\ \mathfrak{b}_2^n,\ \mathbb{A}^n}$

Step 1. Average $\boldsymbol{\mathfrak{b}}^n$ to get $\mathcal{P}$-grid problem: $\boxed{h^n,\ u_1^n,\ u_2^n,\ \mathfrak{B}_1^n,\ \mathfrak{B}_2^n}$

$$\Longrightarrow [\mathfrak{B}_1]^n_{ij} = \tfrac{1}{2}\Big([\mathfrak{b}_1]^n_{i-1/2,j} + [\mathfrak{b}_1]^n_{i+1/2,j}\Big)$$

$$\Longrightarrow [\mathfrak{B}_2]^n_{ij} = \tfrac{1}{2}\Big([\mathfrak{b}_2]^n_{i,j-1/2} + [\mathfrak{b}_2]^n_{i,j+1/2}\Big)$$

Step 2. Solve the SMHD equations on $\mathcal{P}$-grid: $\boxed{h^{n+1},\ u_1^{n+1},\ u_2^{n+1},\ \mathfrak{B}_1^\star,\ \mathfrak{B}_2^\star}$

Step 3. Average $\mathbf{u}^{n+1}$ to get $\mathcal{S}$-grid problem: $\boxed{U_1^\star,\ U_2^\star,\ \mathbb{A}^n}$

$$\Longrightarrow [U_1]^\star_{i,j-1/2} = \tfrac{1}{2}\Big([u_1]^{n+1}_{i,j-1} + [u_1]^{n+1}_{ij}\Big)$$

$$\Longrightarrow [U_2]^\star_{i-1/2,j} = \tfrac{1}{2}\Big([u_2]^{n+1}_{i-1,j} + [u_2]^{n+1}_{ij}\Big)$$

Step 4. Solve induction equation on $\mathcal{S}$-grid: $\boxed{\mathbb{A}^{n+1}}$

$$\Longrightarrow \mathbb{A}^{n+1}_{i-1/2,j-1/2} = \mathbb{A}^n_{i-1/2,j-1/2} - \Delta t\, \Omega^{n+1/2}_{i-1/2,j-1/2}$$

Step 5. Compute $\nabla \times \mathbb{A}$: $\boxed{\mathfrak{b}_1^{n+1},\ \mathfrak{b}_2^{n+1}}$

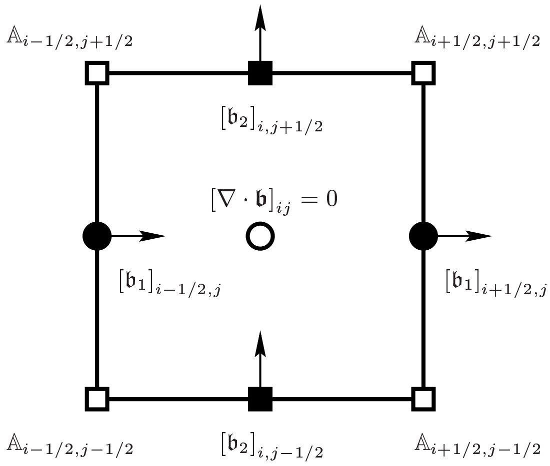

Figure 5.1: Grid staggering for the induction equation.

$$\Longrightarrow [\mathfrak{b}_1]^{n+1}_{i-1/2,j} = \frac{1}{\Delta y}\left(\mathbb{A}^{n+1}_{i-1/2,j+1/2} - \mathbb{A}^{n+1}_{i-1/2,j-1/2}\right)$$

$$\Longrightarrow [\mathfrak{b}_2]^{n+1}_{i,j-1/2} = \frac{1}{\Delta x}\left(\mathbb{A}^{n+1}_{i-1/2,j-1/2} - \mathbb{A}^{n+1}_{i+1/2,j-1/2}\right)$$

In words, the algorithm says that we begin with *primary* quantities h^n, $\mathbf{u}^n$, $\mathfrak{b}^n$, and $\mathbb{A}^n$. The magnetic field is averaged onto the $\mathcal{P}$-grid on which we solve the SMHD equations. The updated $\mathcal{P}$-grid velocities are then averaged onto the $\mathcal{S}$-grid on which the induction equation for the magnetic potential is solved. Finally, the magnetic potential is differenced and we obtain the updated magnetic field values.

In the above description of constrained transport, each step is clearly defined with the exception of **Step 4**. In **Step 4** there are many options for the integration of the induction equation. We consider in detail the approaches of [7, 20, 78] in the next section.

5.4 Methods for integrating the induction equation

The most difficult question in the constrained transport method is the question of how to integrate the induction equation. In particular, the question becomes how to construct the electric field Ω from known information at time $t = t_n$ and $t = t_\star$. In this section we consider the approaches of Dai and Woodward [20], Balsara and Spicer [7], and Ryu, Jones, Miniati, and Frank [78].

5.4.1 The DW scheme

The first CT method we consider is taken from Dai and Woodward [20]. Their updating procedure for the magnetic potential first involves spatially averaging $\mathcal{P}$-grid electric field

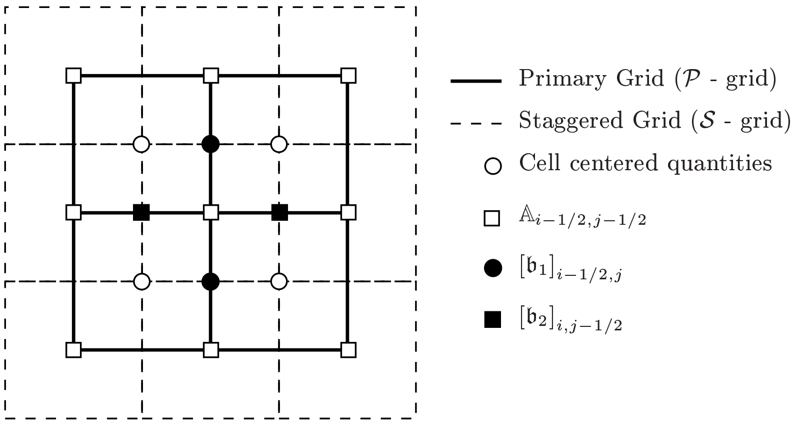

Figure 5.2: Grid staggering for the ideal MHD and SMHD equations.

values to obtain $\mathcal{S}$-grid values. The spatial averaging is done for both the $t = t_n$ values and the $t = t_{n+1}$ values obtained after applying the wave propagation method on the $\mathcal{P}$-grid. These two values are then averaged in time to obtain an approximation to the electric field at $t = t_{n+1/2}$. Mathematically this can be written as

$$\begin{aligned}\Omega^{n+1/2}_{i-1/2,j-1/2} \equiv \frac{1}{2}\Bigg[&\frac{1}{4}\left(\Omega^n_{ij} + \Omega^n_{i-1,j} + \Omega^n_{i,j-1} + \Omega^n_{i-1,j-1}\right) \\ &+\frac{1}{4}\left(\Omega^\star_{ij} + \Omega^\star_{i-1,j} + \Omega^\star_{i,j-1} + \Omega^\star_{i-1,j-1}\right)\Bigg],\end{aligned} \tag{5.31}$$

where $\Omega^n = -u^n_1 \mathfrak{B}^n_2 + u^n_2 \mathfrak{B}^n_1$ is taken from the previous time step and $\Omega^\star = -u^{n+1}_1 \mathfrak{B}^\star_2 + u^{n+1}_2 \mathfrak{B}^\star_1$ is taken from the results of the wave propagation step on the $\mathcal{P}$-grid. This intermediate $\Omega^{n+1/2}$ is then used in the induction equation update (5.24)-(5.26) to obtain $\mathbb{A}^{n+1}$, $\mathfrak{b}^{n+1}_1$, and $\mathfrak{b}^{n+1}_2$.

The accuracy of this scheme suffers from the fact that the update for the magnetic potential is not TVD. This update requires averaging in both space and time; and therefore, can introduce strong spurious oscillations in the vicinity of discontinuities. As an example, we reconsider the 1D SMHD example shown in Chapter 4. We keep the Riemann data aligned with the x-coordinate, but we solve using the 2D wave propagation method with DW constrained transport on a 200×200 grid on the domain $(x, y) \in [-1, 1]$. The results at a $y =$ constant slice are shown in Figure 5.4. These results demonstrate that the DW scheme can produce strong oscillations near discontinuities.

5.4.2 The BS *scheme*

The second CT method we consider is taken from Balsara and Spicer [7]. Their update for the magnetic potential is based on the realization that Ω is proportional to both the 5^{th} component of the flux function in the x-direction and the 4^{th} component of the flux function

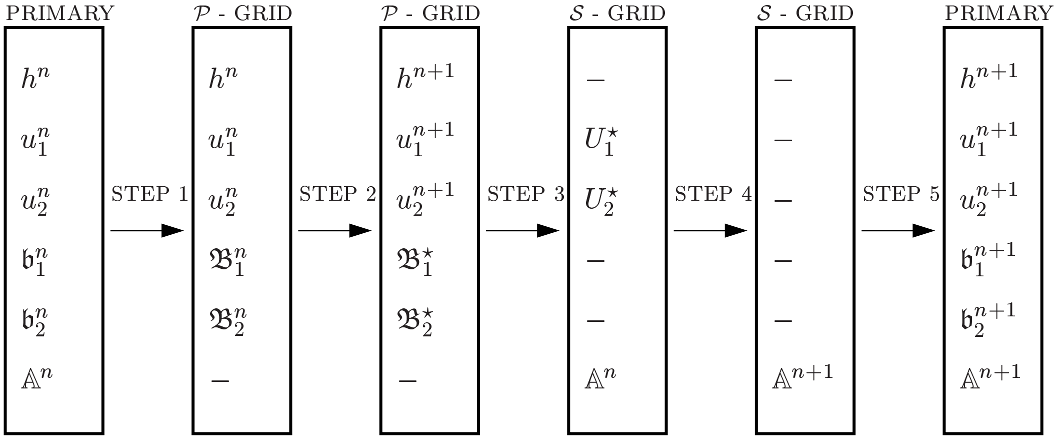

Figure 5.3: Flow chart for the wave propagation method with constrained transport.

in the y-direction:

$$\Omega = -f_5 = g_4 = -u_1\mathfrak{B}_2 + u_2\mathfrak{B}_1\,. \tag{5.32}$$

Furthermore, the wave propagation method produces at each time step numerical approximations to the flux function:

$$[F_5]^{n+1/2}_{i-1/2,j} = -\frac{1}{2}\left(\Omega^n_{ij} + \Omega^n_{i-1,j}\right) + \Phi^x_{i-1/2,j} \tag{5.33}$$

$$[G_4]^{n+1/2}_{i,j-1/2} = +\frac{1}{2}\left(\Omega^n_{ij} + \Omega^n_{i,j-1}\right) + \Phi^y_{i,j-1/2}\,, \tag{5.34}$$

where Φ^x and Φ^y include the *upwind* and the *high-resolution* corrections in the x- and y- directions, respectively. To obtain a value of Ω on the $\mathcal{S}$-grid the following spatial interpolation is applied:

$$\begin{aligned}
\Omega^{n+1/2}_{i-1/2,j-1/2} &\equiv \frac{1}{4}\left([G_4]_{i,j-1/2} + [G_4]_{i-1,j-1/2} - [F_5]_{i-1/2,j} - [F_5]_{i-1/2,j-1}\right) \\
&= \frac{1}{4}\left(\Omega^n_{ij} + \Omega^n_{i-1,j} + \Omega^n_{i,j-1} + \Omega^n_{i-1,j-1}\right) \\
&+ \frac{1}{2}\left[\frac{1}{2}\left(\Phi^y_{i,j-1/2} + \Phi^y_{i-1,j-1/2}\right) - \frac{1}{2}\left(\Phi^x_{i-1/2,j} + \Phi^x_{i-1/2,j-1}\right)\right] \\
&\equiv \bar{\Omega}^n_{i-1/2,j-1/2} + \frac{1}{2}\left(\bar{\Phi}^y_{i-1/2,j-1/2} - \bar{\Phi}^x_{i-1/2,j-1/2}\right)\,.
\end{aligned} \tag{5.35}$$

This intermediate $\Omega^{n+1/2}$ is then used in the induction equation update (5.24)-(5.26) to obtain $\mathbb{A}^{n+1}$, $\mathfrak{b}_1^{n+1}$, and $\mathfrak{b}_2^{n+1}$.

5.4.3 The RMJF *scheme*

The third CT method we consider is taken from Ryu, Miniati, Jones, and Frank [78]. This method, as formulated in [78] and [90] approximates the $\mathcal{S}$-grid value for Ω via the following

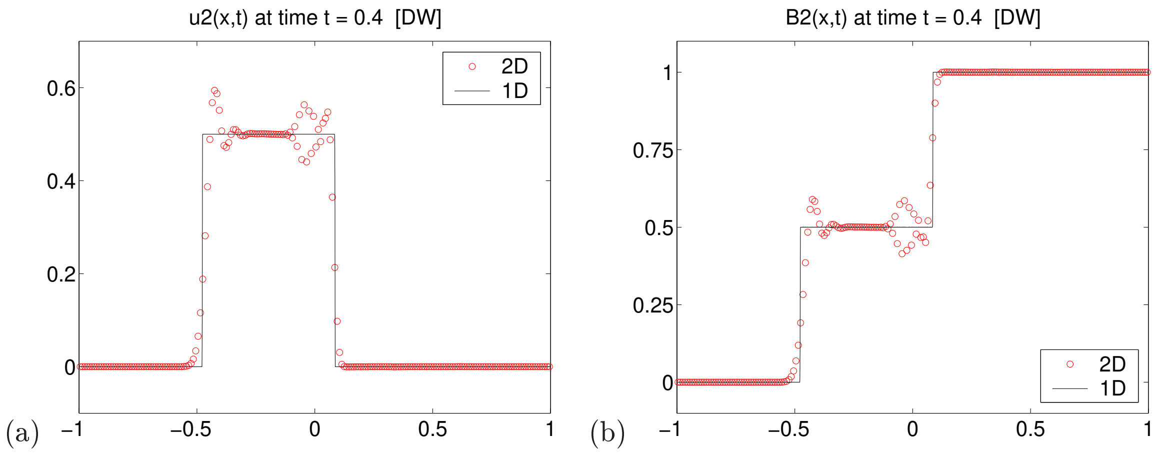

Figure 5.4: The same 1D SMHD example as shown in Chapter 4, but solved using the the DW scheme on a 200×200 grid with a Courant number of 0.9. In this figure we have plotted a $y =$ constant slice of the y-components of (a) the velocity and (b) the magnetic field. Note the spurious oscillations produced near discontinuities.

formula:

$$\Omega^{n+1/2}_{i-1/2,j-1/2} \equiv \frac{1}{2}\left(\left[\check{G}_4\right]_{i,j-1/2} + \left[\check{G}_4\right]_{i-1,j-1/2} - \left[\check{F}_5\right]_{i-1/2,j} - \left[\check{F}_5\right]_{i-1/2,j-1} \right), \tag{5.36}$$

where

$$\left[\check{F}_5\right]_{i-1/2,j} \equiv \frac{1}{2}\left([u_1\mathfrak{B}_2]^n_{ij} + [u_1\mathfrak{B}_2]^n_{i-1,j} \right) + \Phi^x_{i-1/2,j} \tag{5.37}$$

$$\left[\check{G}_4\right]_{i,j-1/2} \equiv \frac{1}{2}\left([u_2\mathfrak{B}_1]^n_{ij} + [u_2\mathfrak{B}_1]^n_{i-1,j} \right) + \Phi^y_{i,j-1/2}\,. \tag{5.38}$$

The motivation for this update is that when either $\partial_x q \equiv 0$ or $\partial_y q \equiv 0$, the RMJF scheme exactly reduces to the 1D wave propagation scheme (see Toth [90]). Plugging definitions (5.37) and (5.38) back into (5.36) and making use of Ohm's law (5.23) yields an equivalent formulation:

$$\begin{aligned} \Omega^{n+1/2}_{i-1/2,j-1/2} &\equiv \frac{1}{4}\left(\Omega^n_{ij} + \Omega^n_{i-1,j} + \Omega^n_{i,j-1} + \Omega^n_{i-1,j-1}\right) \\ &+ \frac{1}{2}\left(\Phi^y_{i,j-1/2} + \Phi^y_{i-1,j-1/2}\right) - \frac{1}{2}\left(\Phi^x_{i-1/2,j} + \Phi^x_{i-1/2,j-1}\right) \\ &\equiv \bar{\Omega}^n_{i-1/2,j-1/2} + \bar{\Phi}^y_{i-1/2,j-1/2} - \bar{\Phi}^x_{i-1/2,j-1/2}\,. \end{aligned} \tag{5.39}$$

This method is identical to the BS scheme with the exception that the RMJF scheme adds approximate values of both Φ^x and Φ^y into the update, while the BS scheme averages these two values. In this formulation it is clear that when either Φ^x or Φ^y are identically zero, the RMJF scheme will reduce to the 1D wave propagation method. In these cases the extra averaging in the BS scheme is not needed. In fact, this inconsistency is pointed out by Balsara and Spicer [7] and a kind of *multidimensional limiter* is proposed to correct this problem. In the next section, however, we show that neither the RMJF nor the BS scheme are consistent methods in general. The multidimensional limiter proposed in [7] does not correct this problem.

5.4.4 Inconsistency of the BS *and* RMJF *schemes*

The BS and RMJF schemes are essentially the same approach but with different choices for how much of the upwind corrections are added into the update. Because the Φ's in general contain $\mathcal{O}(1)$ corrections, it is clear that something must be wrong with either the BS or the RMJF update. In fact, both are inconsistent. To analyze this in more detail, let us compare the BS and RMJF schemes to the numerically consistent wave propagation method without constrained transport.

Claim 5.4.1 *The Balsara and Spicer scheme [7] and the Ryu, Miniati, Jones, and Frank scheme [78] are inconsistent numerical methods.*

Proof. The component of the numerical flux function used in the update for $\mathfrak{B}_1$ generated by the wave propagation method without constrained transport (i.e., the base scheme) is given by

$$F_{\text{BASE}} = \frac{1}{2}\left(\Omega^n_{i,j+1} + \Omega^n_{ij}\right) + \Phi^y_{i,j+1/2}\,. \tag{5.40}$$

The corresponding numerical flux function using either BS ($\alpha = 1/2$) or RMJF ($\alpha = 1$) is given by

$$\begin{aligned} F_{\text{CT}} =& \frac{1}{2}\left(\bar{\Omega}^n_{i+1/2,j+1/2} + \bar{\Omega}^n_{i-1/2,j+1/2}\right) + \frac{\alpha}{2}\left(\bar{\Phi}^y_{i+1/2,j+1/2} + \bar{\Phi}^y_{i-1/2,j+1/2}\right) \\ &- \frac{\alpha}{2}\left(\bar{\Phi}^x_{i+1/2,j+1/2} + \bar{\Phi}^x_{i-1/2,j+1/2}\right) \\ \equiv& \frac{1}{2}\left(\bar{\Omega}^n_{i+1/2,j+1/2} + \bar{\Omega}^n_{i-1/2,j+1/2}\right) + \alpha\bar{\bar{\Phi}}^y_{i,j+1/2} - \alpha\bar{\bar{\Phi}}^x_{i,j+1/2}\,. \end{aligned} \tag{5.41}$$

Subtracting these expressions, we find that to leading order

$$F_{\text{BASE}} - F_{\text{CT}} \sim \Phi^y_i - \alpha\bar{\bar{\Phi}}^y_i + \alpha\bar{\bar{\Phi}}^x_i + \dots \quad . \tag{5.42}$$

We first note that in general Φ^y_i, $\bar{\bar{\Phi}}^y_i$, and $\bar{\bar{\Phi}}^x_i$ are all $\mathcal{O}(1)$ quantities. From this we can see that in general (i.e., $\bar{\bar{\Phi}}^y_i \neq 0$ and $\bar{\bar{\Phi}}^x_i \neq 0$) all choices of α result in

$$F_{\text{BASE}} - F_{\text{CT}} \sim \mathcal{O}(1)\,. \tag{5.43}$$

Because the base scheme is a consistent numerical method (see LeVeque [53]), the above analysis shows that neither the BS scheme nor the RMJF scheme are consistent methods for solving the SMHD and ideal MHD equations. ■

5.5 MPACT*: a new constrained transport method*

On the one hand, the constrained transport approach seems like a attractive alternative to methods based on solving additional non-hyperbolic equations (the projection method and the divergence cleaning method) and methods based on modifying the governing equations (the 8-wave formulation and the divergence cleaning method). On the other hand, the three methods described above for computing the electric field produce either an update with spurious oscillations in the case of the DW scheme or an inconsistent update in the case of the BS and RMJF schemes. In this section we introduce a novel approach for computing the electric field that will be shown to produce a consistent and significantly less oscillatory numerical update.

5.5.1 The magnetic potential equation

From Faraday's law we have shown in Section 5.3 that the magnetic potential obeys an equation of the form

$$\partial_t \mathbb{A} + \Omega = \partial_t \mathbb{A} - u_1 \mathfrak{B}_2 + u_2 \mathfrak{B}_1 = 0\,. \tag{5.44}$$

If in this equation we replace the magnetic field by the appropriate derivatives of the magnetic potential ($\mathfrak{B} = \nabla \times \mathbb{A}$), then we obtain

$$\partial_t \mathbb{A} + u_1 \partial_x \mathbb{A} + u_2 \partial_y \mathbb{A} = 0\,. \tag{5.45}$$

This is an advection equation (see Section 2.5) and is linear and strictly hyperbolic for all $(u_1, u_2)^t \in \mathbb{R} \times \mathbb{R}$. In this section we introduce a new constrained transport method based on coupling the numerical update for the magnetohydrodynamic equations with an update for the magnetic potential equation (5.45). Because this method is based on the advection of the magnetic potential, we refer to this scheme as the MPACT (Magnetic Potential Advection Constrained Transport) scheme.

5.5.2 An operator splitting approach

By writing the full magnetic potential equation for the magnetic potential we are now able to update the magnetic potential given a velocity field. We have thus removed the need for artificially *constructing* an electric field. The simplest way to solve both the ideal MHD or SMHD and the magnetic potential equation is by operator splitting techniques. The two operators are

$$\begin{aligned} \mathcal{L}_1 &\equiv \text{ the ideal MHD or SMHD equations} \\ \mathcal{L}_2 &\equiv \text{ the magnetic potential equation (5.45).} \end{aligned}$$

Step 2 and **Step 4** in the constrained transport method as outlined in Section 5.3.3 can now be written as

$$\begin{aligned} &\textbf{Step 2:} \text{ (full step with } \mathcal{L}_1) \quad & q^\star &= \mathcal{L}_1^{\Delta t} q^n \\ &\textbf{Step 4:} \text{ (full step with } \mathcal{L}_2) \quad & q^{n+1} &= \mathcal{L}_2^{\Delta t} q^\star\,. \end{aligned}$$

The update involving the operator $\mathcal{L}_1$ is done with the wave propagation method from Chapter 2. We address the question of how to update the magnetic potential in the next section.

5.5.3 Keeping the magnetic field non-oscillatory

Although the magnetic potential equation (5.45) is a simple advection equation, care must be taken when solving this equation. We would like to apply the wave propagation method for the advection equation (see Chapter 2), in which case wave limiters would be applied to the solution of $\mathbb{A}$. At the end of the day, however, we are interested in ensuring a non-oscillatory magnetic field. This is not guaranteed by applying limiters to only $\mathbb{A}$. One option would be to apply limiters when differencing the magnetic potential:

$$\mathfrak{B} = \nabla \times \mathbb{A}. \tag{5.46}$$

This is in general a bad idea since we require *central* finite difference operators when approximating $\mathfrak{B} = \nabla \times \mathbb{A}$ in order for the exact divergence-free condition to hold.

Instead, we propose in this work an alternative approach based on composite schemes [61]. The idea is to add a judicious amount of diffusion into the solution of the magnetic potential equation so that the magnetic field remains non-oscillatory, but the shock capturing ability of the wave propagation method is not destroyed. Therefore, we replace **Step 4** above by a partial diffusive Godunov step and a partial high-resolution wave propagation step:

Step 4a: (partial step with Godunov) $\quad q^{n+\alpha} = \mathcal{L}_2^{\alpha\Delta t} q^\star$

Step 4b: (partial step with Wave Propagation) $\quad q^{n+1} = \mathcal{L}_2^{(1-\alpha)\Delta t} q^{n+\alpha}\,,$

where $0 \leq \alpha \leq 1$. We have found in numerical experiments that a value of $\alpha = 0.3$ gives a good balance between shock resolution and oscillation reduction.

5.5.4 A note about 3D

How does this method generalize to three space dimensions? In 3D the necessary grid staggering required to keep the magnetic field divergence-free is shown in Figure 5.5. The magnetic potential in 3D obeys a generalized version of equation (5.45). In order to obtain this equation, we apply the following manipulations to Faraday's law:

$$\begin{aligned}
&\partial_t \mathbf{B} + \nabla \times (\mathbf{B} \times \mathbf{u}) = 0 \\
\Longrightarrow\quad &\partial_t (\nabla \times \mathbb{A}) + \nabla \times [(\nabla \times \mathbb{A}) \times \mathbf{u}] = 0 \\
\Longrightarrow\quad &\partial_t \mathbb{A} + (\nabla \times \mathbb{A}) \times \mathbf{u} = 0 \\
\Longrightarrow\quad &\partial_t \mathbb{A} + (\nabla \times \mathbb{A}) \times \mathbf{u} = \mathbf{u}\,(\nabla \cdot \mathbb{A})\,. \qquad \text{(Gauge condition)}
\end{aligned}$$

Taking the last expression above and expanding in individual components yields a magnetic potential equation of the form

$$\partial_t \begin{bmatrix} \mathbb{A}_1 \\ \mathbb{A}_2 \\ \mathbb{A}_3 \end{bmatrix} + M_1\, \partial_x \begin{bmatrix} \mathbb{A}_1 \\ \mathbb{A}_2 \\ \mathbb{A}_3 \end{bmatrix} + M_2\, \partial_y \begin{bmatrix} \mathbb{A}_1 \\ \mathbb{A}_2 \\ \mathbb{A}_3 \end{bmatrix} + M_3\, \partial_z \begin{bmatrix} \mathbb{A}_1 \\ \mathbb{A}_2 \\ \mathbb{A}_3 \end{bmatrix} = 0\,, \tag{5.47}$$

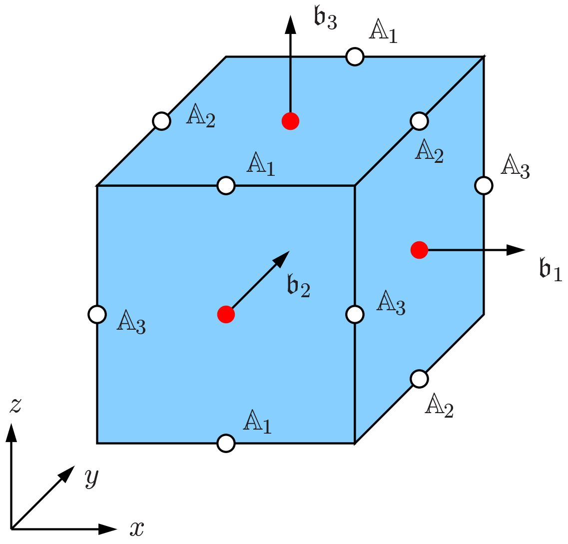

Figure 5.5: The grid staggering for the ideal MHD equations in three space dimensions.

where

$$M_1 \equiv \begin{bmatrix} -u_1 & -u_2 & -u_3 \\ -u_2 & u_1 & 0 \\ -u_3 & 0 & u_1 \end{bmatrix}, \quad M_2 \equiv \begin{bmatrix} u_2 & -u_1 & 0 \\ -u_1 & -u_2 & -u_3 \\ 0 & -u_3 & u_2 \end{bmatrix}, \quad \text{and} \quad M_3 \equiv \begin{bmatrix} u_3 & 0 & -u_1 \\ 0 & u_3 & -u_2 \\ -u_1 & -u_2 & -u_3 \end{bmatrix}.$$

This system is linear and hyperbolic; and therefore, represents only a minor complication over the advection equation that $\mathbb{A}$ obeys in two space dimensions.

The strategy we propose in three dimensions is to average to the flux Jacobians from (5.47) (i.e., average the fluid velocities) in the following way:

$$[M_1]_{i,j-1/2,k-1/2} = \frac{1}{4}\Big([M_1]_{ijk} + [M_1]_{i,j-1,k} + [M_1]_{i,j,k-1} + [M_1]_{i,j-1,k-1}\Big) \tag{5.48}$$

$$[M_2]_{i-1/2,j,k-1/2} = \frac{1}{4}\Big([M_2]_{ijk} + [M_2]_{i-1,j,k} + [M_2]_{i,j,k-1} + [M_2]_{i-1,j,k-1}\Big) \tag{5.49}$$

$$[M_3]_{i-1/2,j-1/2,k} = \frac{1}{4}\Big([M_3]_{ijk} + [M_3]_{i,j-1,k} + [M_3]_{i-1,j,k} + [M_3]_{i-1,j-1,k}\Big). \tag{5.50}$$

Having applied the necessary averaging, the 3D magnetic potential equation (5.47) can be solved for $\mathbb{A}$ at at cell corners. Once the solution has been computed, the components as shown in Figure 5.5 can be obtained by appropriately averaging $\mathbb{A}$:

$$[\mathbb{A}_1]_{i,j-1/2,k-1/2} = \frac{1}{2}\Big([\mathbb{A}_1]_{i-1/2,j-1/2,k-1/2} + [\mathbb{A}_1]_{i+1/2,j-1/2,k-1/2}\Big) \tag{5.51}$$

$$[\mathbb{A}_2]_{i-1/2,j,k-1/2} = \frac{1}{2}\Big([\mathbb{A}_2]_{i-1/2,j-1/2,k-1/2} + [\mathbb{A}_2]_{i-1/2,j+1/2,k-1/2}\Big) \tag{5.52}$$

$$[\mathbb{A}_3]_{i-1/2,j-1/2,k} = \frac{1}{2}\Big([\mathbb{A}_3]_{i-1/2,j-1/2,k-1/2} + [\mathbb{A}_3]_{i-1/2,j-1/2,k+1/2}\Big). \tag{5.53}$$

Table 5.1: Total variation for the base, RMJF, BS, DW, and MPACT schemes for a coordinate aligned SMHD Riemann problem.

	TOTAL VARIATION IN u_2			
method	base/RMJF	BS	DW	MPACT
at $t=0$	0.000000	0.000000	0.000000	0.000000
100×100	1.001146	1.504930	2.182742	1.073761
200×200	1.000363	1.802036	2.294090	1.048190
400×400	1.000138	2.471619	2.388129	1.031517

The above proposed method in 3D exactly reduces to the 2D MPACT scheme.

5.6 Test problems in 2D

In this section we test the MPACT against the standard cell centered wave propagation method, the DW scheme, the BS scheme, and the RMJF scheme. We refer to the wave propagation method without constrained transport as the base scheme.

5.6.1 SMHD test: coordinate aligned shock

The first test we consider is the coordinate aligned shock tube problem from Chapter 4. We solve this problem on the domain $(x, y) \in [-1, 1] \times [-1, 1]$ with 200×200 points. The initial magnetic potential is given by

$$\mathbb{A}(x, y, 0) = \begin{cases} y+1 & \text{if} \quad x \leq 0 \\ y - 2x + 1 & \text{if} \quad x \geq 0\,. \end{cases} \tag{5.54}$$

The solution for the MPACT scheme at a y = constant slice is shown in Figure 5.6. We note that the MPACT scheme slightly smears the linear discontinuities in $u_2(x, y, t)$ and $B_2(x, y, t)$ and introduces small oscillations into the $u_2(x, y, t)$ profile.

These solutions are not as good as the base scheme. However, we will show in subsequent examples that in a truly multidimensional problem, the MPACT scheme is much more robust than the base scheme. Furthermore, in Table 5.1 we compute the total variation of u_2 for different grid resolutions. This study shows that the MPACT scheme stays much closer to the total variation of the base scheme solution than the BS and the DW schemes. As predicted in Claim 5.4.1, the BS scheme is inconsistent on this problem. The DW scheme is consistent, but suffers from the generation of large unphysical oscillations.

5.6.2 SMHD test: multidimensional steady-state shock

We now consider an example from De Sterck [84] in order to test the robustness of constrained transport on a multidimensional flow. The computational domain is the square

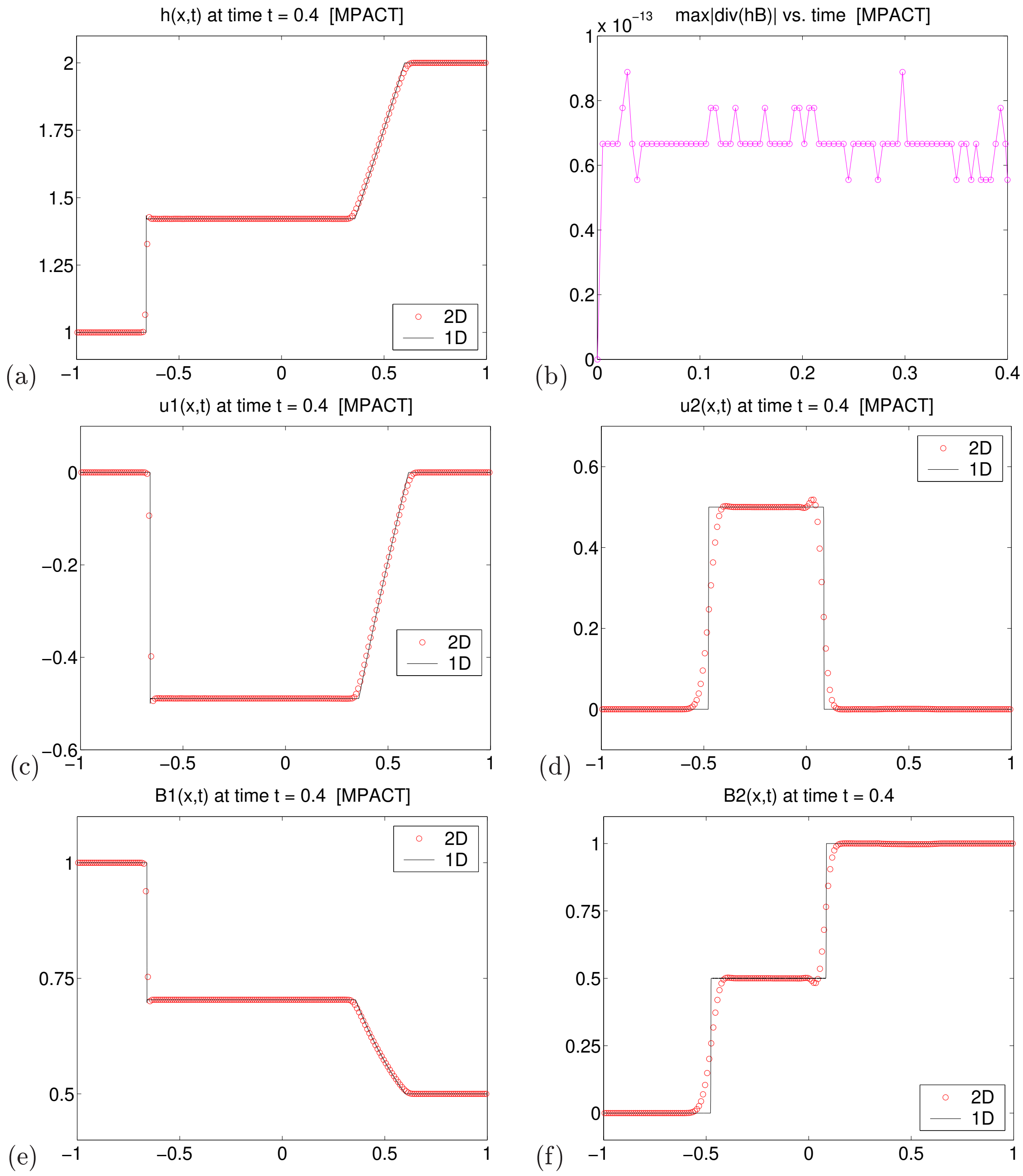

Figure 5.6: The same 1D SMHD example as shown in Chapter 4, but solved using the the MPACT scheme on a 200×200 grid. In this figure we have plotted a $y =$ constant slice of each variable.

Table 5.2: Time of crash for various schemes on a multidimensional SMHD shock problem.

METHOD	TIME OF CRASH
base scheme*	$t = 0.0336$
RMJF scheme†	$t = 0.0347$
BS scheme†	$t = 0.0590$
DW scheme*	$t = 0.4583$
MPACT scheme*	–

*Transverse corrections, CFL = 0.9
†No transverse corrections, CFL = 0.45

box $(x, y) \in [-1, 1] \times [-1, 1]$. The initial conditions are taken as

$$\vec{v}\,(x, y, 0) = \begin{cases} \vec{v}_< & \text{if} \quad y < 0 \\ \vec{v}_> & \text{if} \quad y > 0\,, \end{cases} \tag{5.55}$$

where

$$\vec{v}_< = \begin{bmatrix} h \\ u_1 \\ u_2 \\ B_1 \\ B_2 \end{bmatrix}_< = \begin{bmatrix} 1 \\ 4.5 \\ 0 \\ 2 \\ 0 \end{bmatrix} \quad \text{and} \quad \vec{v}_> = \begin{bmatrix} h \\ u_1 \\ u_2 \\ B_1 \\ B_2 \end{bmatrix}_> = \begin{bmatrix} 2 \\ 5.5 \\ 0 \\ 0.5 \\ 0 \end{bmatrix}. \tag{5.56}$$

The boundary conditions on the top, bottom, and right sides are set to outflow, while at the left boundary we impose an inflow condition given by

$$\vec{v}\,(-1, y, t) = \begin{cases} \vec{v}_< & \text{if} \quad y < 0 \\ \vec{v}_> & \text{if} \quad y > 0\,, \end{cases} \tag{5.57}$$

where $\vec{v}_<$ and $\vec{v}_>$ are again given by (5.56). The initial magnetic potential is

$$\mathbb{A}(x, y, 0) = \begin{cases} 2y + 2 & \text{if} \quad y \leq 0 \\ y + 2 & \text{if} \quad y \geq 0\,. \end{cases} \tag{5.58}$$

The computation is run until time $t = 1$, at which point the system has reached its steady-state.

The base, DW, BS, and RMJF schemes were also tested on this problem. However, these methods all crash at various points in the calculation because they produce negative heights (see Table 5.2). The base scheme crashes because $\nabla \cdot \mathfrak{B}$ becomes very large near the singularity at $(x, y) = (-1, 0)$. The DW scheme crashes because large unphysical oscillations are generated across the multidimensional shock. The BS and RMJF schemes crash because they are inconsistent methods on this multidimensional test problem. The results from the MPACT scheme are shown in Figure 5.7 and compare well to the results found in [84].

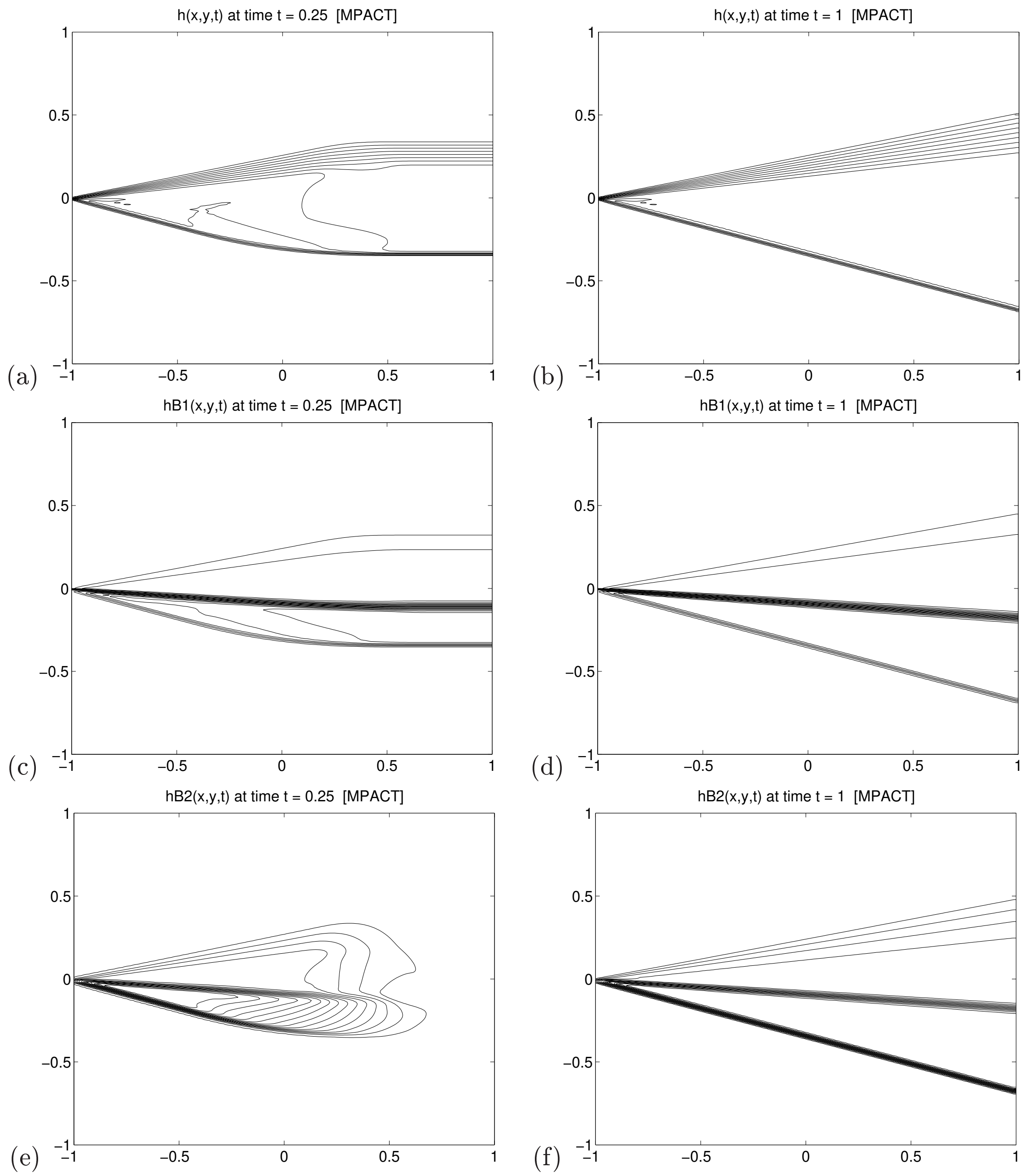

Figure 5.7: Solution obtained from the MPACT scheme for the multidimensional shock problem. Shown are the height at time (a) $t = 0.25$ and (b) $t = 1.0$, $\mathfrak{B}_1$ at time (c) $t = 0.25$ and (d) $t = 1.0$, and $\mathfrak{B}_2$ at time (e) $t = 0.25$ and (f) $t = 1.0$.

In order to better quantify the performance of the 2D MPACT scheme, we consider the steady state SMHD equations:

$$\partial_x \underbrace{\begin{bmatrix} hu_1 \\ hu_1^2 - hB_1^2 + \frac{1}{2}gh^2 \\ hu_1u_2 - hB_1B_2 \\ hB_1 \end{bmatrix}}_{q(y,x)} + \partial_y \underbrace{\begin{bmatrix} hu_2 \\ hu_1u_2 - hB_1B_2 \\ hu_2^2 - hB_2^2 + \frac{1}{2}gh^2 \\ hB_2 \end{bmatrix}}_{f(q(y,x))} = 0 \tag{5.59}$$

$$hu_2B_1 - hu_1B_2 = c_0\,. \tag{5.60}$$

These equations can be solved by treating (5.59) as a 1D "time" dependent equation where x is the time-like coordinate and y is the space-like coordinate. The inflow conditions at $x = -1$ act as "initial conditions" for this system. We can solve this equation using the local Lax-Friedrichs method (2.78) from Chapter 2. We take

$$a_{i-1/2} \equiv \max\left(\left| \frac{B_1B_2 - u_1u_2 \pm \sqrt{h\left(u_1^2 - B_1^2 - h + u_2^2 - B_2^2\right)}}{h + B_1^2 - u_1^2} \right| \right) \tag{5.61}$$

and compute on a grid with 20,000 points. In order to obtain the primitive variables (h, u_1, u_2, B_1, B_2) from the conserved variables, we must solve the following nonlinear algebraic equation at each time step:

$$\begin{bmatrix} q_1 \\ q_2 \\ q_3 \\ q_4 \\ c_0 \end{bmatrix} = \begin{bmatrix} hu_1 \\ hu_1^2 - hB_1^2 + \frac{1}{2}gh^2 \\ hu_1u_2 - hB_1B_2 \\ hB_1 \\ hu_2B_1 - hu_1B_2 \end{bmatrix}. \tag{5.62}$$

This 1D solution is compared to an $x =$ constant slice of the 2D MPACT calculation in Figure 5.8. This calculation demonstrates the robustness and accuracy of the MPACT scheme on a 2D SMHD example.

5.6.3 Why do the RMJF, BS, *and* DW *schemes work so poorly on SMHD?*

We made the claim in Chapter 4 that the SMHD equations are not only important for modeling, but also as a good starting point for developing numerical methods for ideal MHD. We argued that the eigensystem for the SMHD is simpler than for ideal MHD and that SMHD does not encounter numerical difficulties when the equations become non-strictly hyperbolic. Why then do the RMJF, BS, and DW methods work so poorly on these equations?

Some discussions of the inconsistency of the RMJF and BS schemes already exist in the literature (see [7, 63, 78]). The problem of spurious oscillations for the DW scheme is briefly discussed in [90]. Despite these shortcomings, however, all of these methods have been applied to ideal MHD flows and have produced seemingly reasonable results. Again: why do the SMHD equations cause so much trouble?

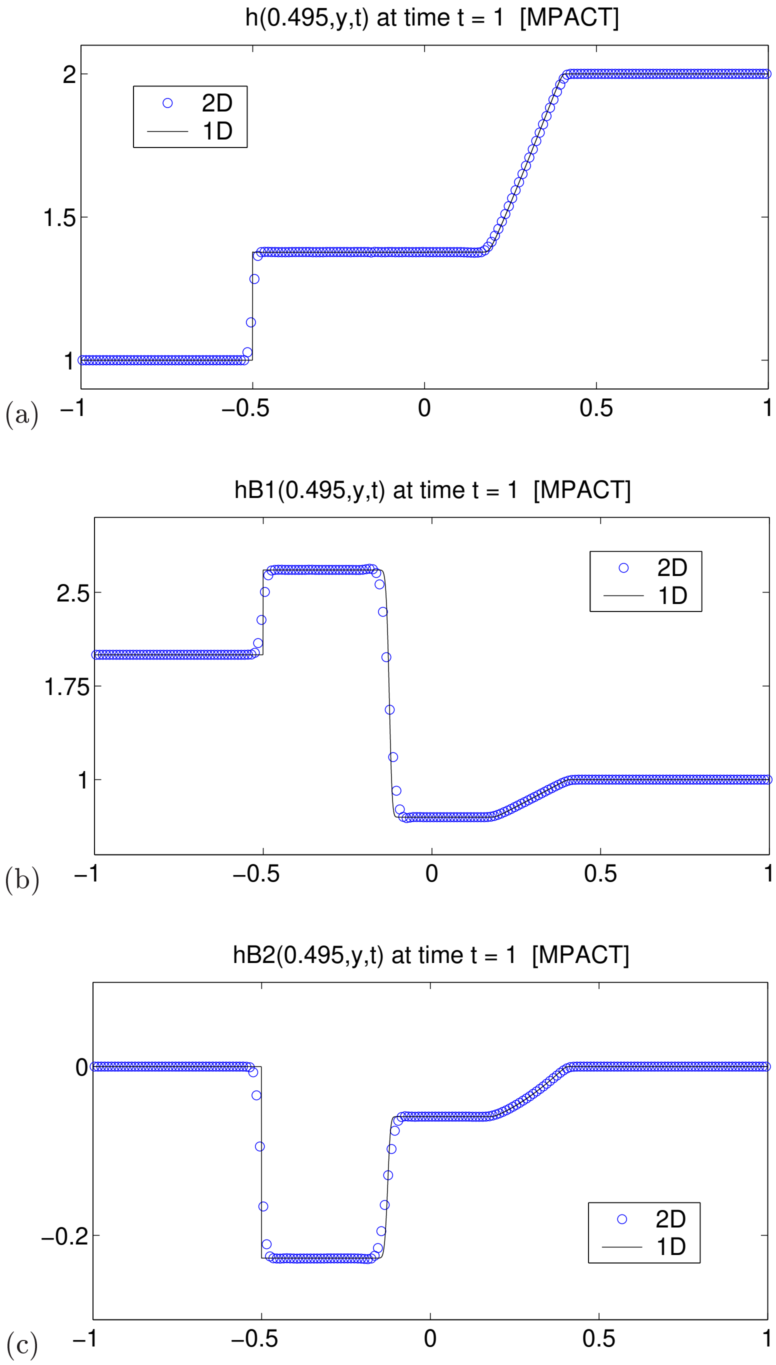

Figure 5.8: An $x =$ constant slice of the 2D solution shown in Figure 5.7 compared against a 1D solution of the steady-state equations.

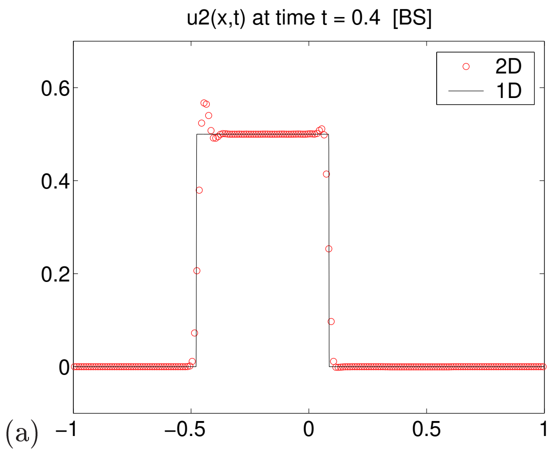

Figure 5.9: The same 1D SMHD example as shown in Chapter 4, but solved using the the BS scheme on a 200×200 grid. In this figure we have plotted the solution using two different Courant numbers: (a) 0.45 and (b) 0.045.

The answer to this question lies in the Courant number. Constrained transport is a process which occurs on the time scale of the fluid velocity ($\mathbf{u}$):

$$\partial_t \mathbb{A} + u_1 \partial_x \mathbb{A} + u_2 \partial_y \mathbb{A} = 0 \,. \tag{5.63}$$

In MHD, the fast magnetosonic waves propagate on a time scale much faster than the fluid velocity, and thus, these waves dictate the time step restrictions necessary for a stable numerical update. This implies that a significant amount of numerical diffusion is added to the much slower waves in the MHD system. In SMHD, the fastest waves are the magnetogravity waves which propagate much slower than the fast magnetosonic waves. This implies that less numerical diffusion is being added to the constrained transport part of the update. Therefore, any problems that occur due to constrained transport are significantly enhanced by the SMHD equations. One would have to go to very high resolutions in the MHD equations to see the errors that are evident in the SMHD system.

To demonstrate the above claim, we re-run the coordinate aligned shock example from Section 5.6.1 using the BS scheme. In particular, we compare the solution using two different Courant numbers: 0.45 and 0.045. The results of these computations are shown in Figure 5.9(a) and 5.9(b), respectively. The plot in Figure 5.9(a) agrees with the results reported in Table 5.1, while the plot in 5.9(b) is much more reminiscent of the numerical errors introduced by constrained transport applied to the ideal MHD equations (see [78, 90]). This result clearly shows that if more numerically averaging is applied to the constrained transport update, then the inconsistencies of the BS and RMJF schemes become much less pronounced.

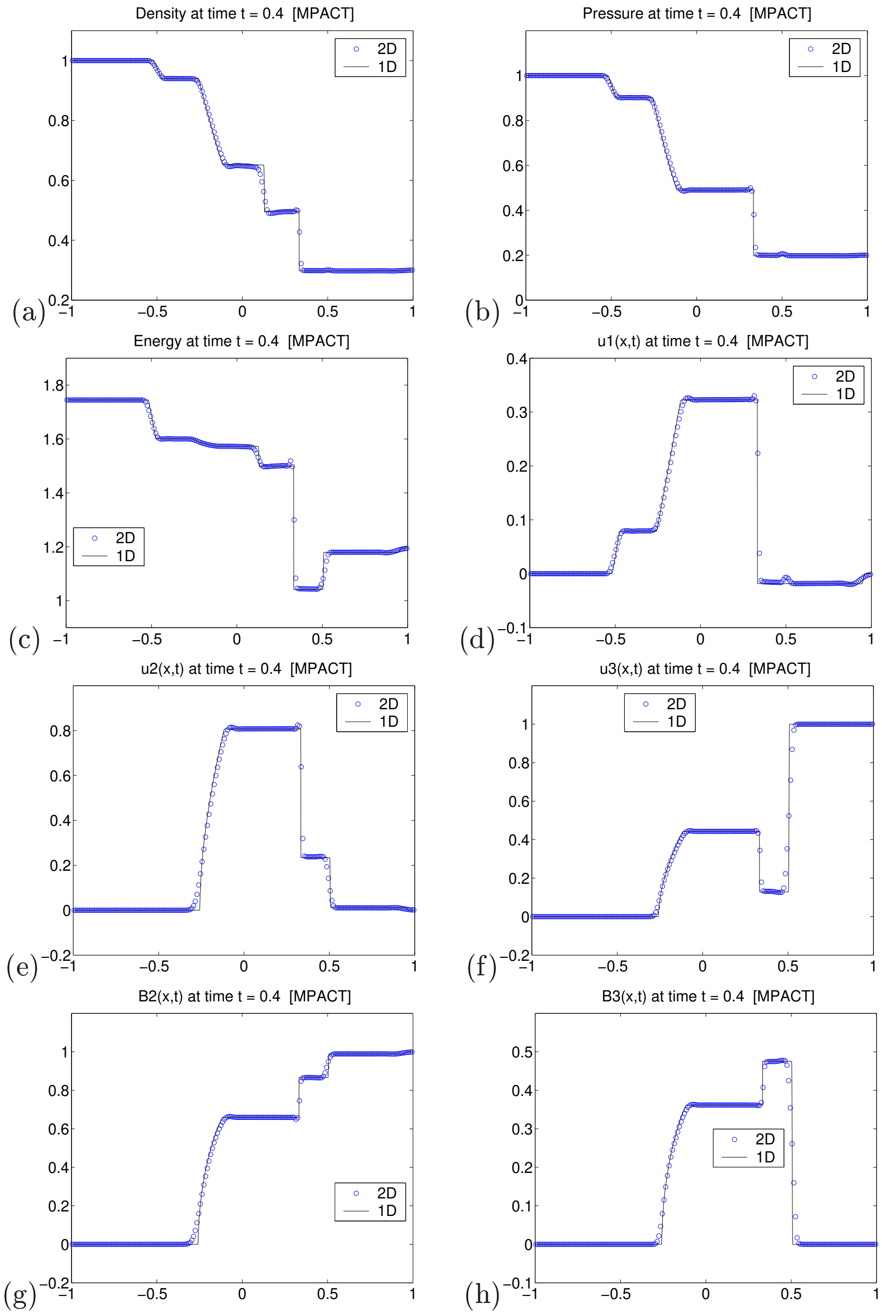

Figure 5.10: The same 1D ideal MHD example as shown in Chapter 3, but solved using the the MPACT scheme on a 200×200 grid. In this figure we have plotted a $y =$ constant slice of each variable.

Table 5.3: Total variation for the base, RMJF, BS, DW, and MPACT schemes for a coordinate aligned ideal MHD Riemann problem.

	TOTAL VARIATION IN $\mathcal{E}$			
method	base/RMJF	BS	DW	MPACT
at $t = 0$	0.550000	0.550000	0.550000	0.550000
100×100	0.861355	0.940561	1.078009	0.9172071
200×200	0.864038	0.977479	1.052223	0.9060817
400×400	0.863602	1.111750	1.049400	0.8937055

5.6.4 Ideal MHD test: coordinate aligned shock

As was the case for SMHD, we first consider a coordinate aligned shock for the ideal MHD equations. We apply the four constrained transport methods to the problem from Chapter 3. We solve this problem on the domain $(x, y) \in [-1, 1] \times [-1, 1]$ with 200×200 points and $\gamma = 5/3$. The initial magnetic potential is

$$\mathbb{A}(x, y, 0) = \begin{cases} 0.7y & \text{if} \quad x \leq 0 \\ 0.7y - x & \text{if} \quad x \geq 0\,. \end{cases} \tag{5.64}$$

The solution for the MPACT scheme at a $y =$ constant slice is shown in Figure 5.10. We also compute the total variation in the total energy ($\mathcal{E}$) for the four constrained transport methods and the base scheme in Table 5.3. As in the SMHD example, the MPACT performs much better than the other constrained transport methods but not as well as the base scheme.

5.6.5 Ideal MHD test: the Orszag-Tang vortex

Next we consider a problem that appears several times in the literature including in [20, 90, 91, 94]. The computational domain in this case is $(x, y) \in [0, 2\pi] \times [0, 2\pi]$ with periodic boundary conditions on all four sides. The initial conditions are given by

$$\rho(x, y, 0) = \gamma^2 \tag{5.65}$$
$$u_1(x, y, 0) = -\sin(y) \tag{5.66}$$
$$u_2(x, y, 0) = \sin(x) \tag{5.67}$$
$$p(x, y, 0) = \gamma \tag{5.68}$$
$$B_1(x, y, 0) = -\sin(y) \tag{5.69}$$
$$B_2(x, y, 0) = \sin(2x) \tag{5.70}$$
$$\mathbb{A}(x, y, 0) = \cos(y) + \frac{1}{2}\cos(2x)\,, \tag{5.71}$$

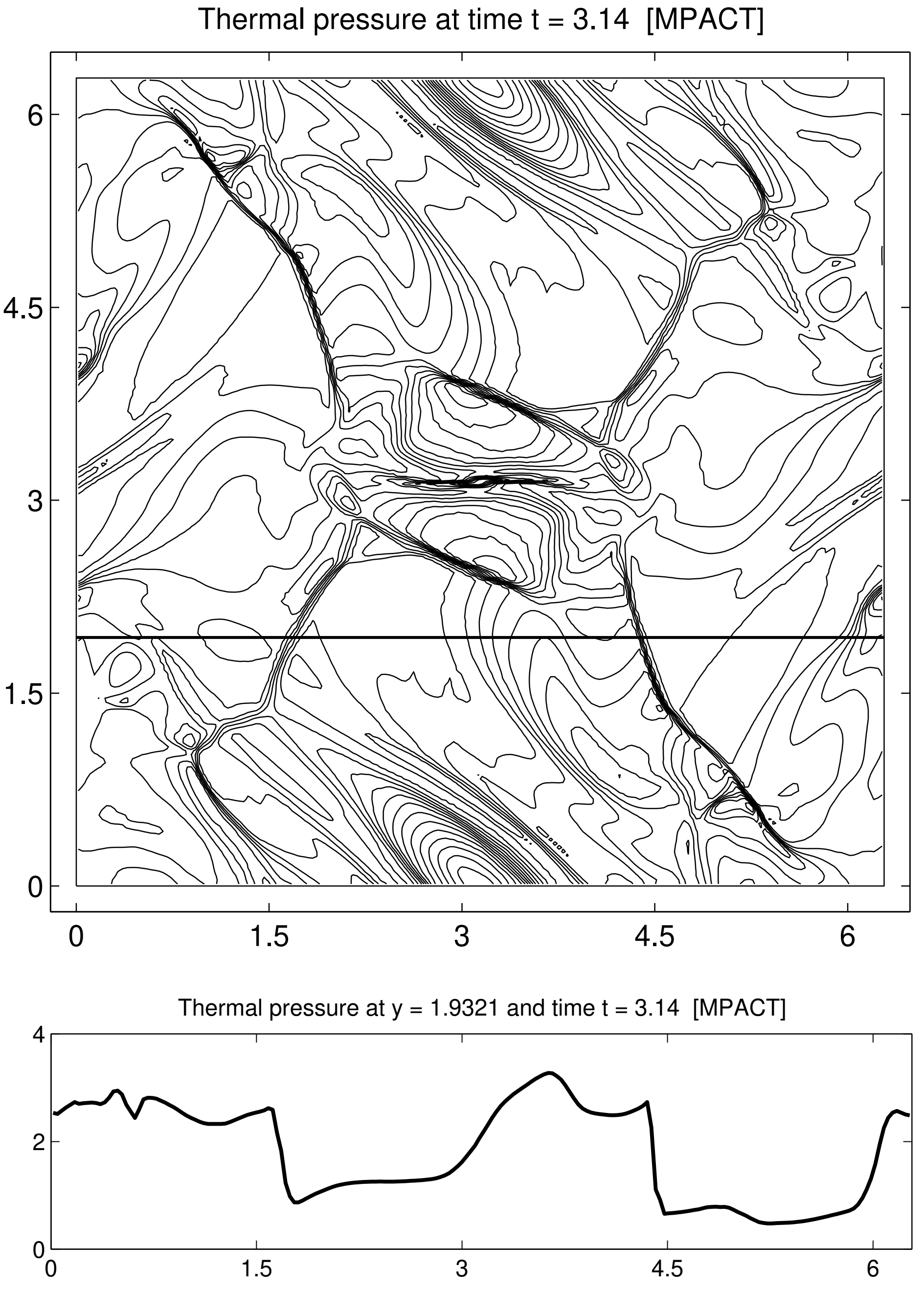

(a)

(b)

Figure 5.11: The Orzsag-Tang vortex test problem for the ideal MHD equations. Shown are (a) a contour plot of the thermal pressure at time $t = 3.14$ and (b) a slice of this data at $y = 1.9321$. The line drawn across the contour plot (a) is the $y = 1.9321$ line.

where $\gamma = 5/3$ and $u_3 = B_3 = 0$. The initial magnetic potential is given by

$$\mathbb{A}(x, y, 0) = \frac{1}{2}\cos(2x) + \cos(y)\,. \tag{5.72}$$

A contour plot of the thermal pressure at time $t = 3.14$ predicted by the MPACT scheme on a 200×200 grid is shown in Figure 5.11(a). A slice of this solution at $y = 1.9321$ is shown in Figure 5.11(b). Although each paper displays the solution at slightly different times and resolutions, our results compare well with those given in [20, 90, 91, 94].

5.6.6 Ideal MHD test: cloud-shock interaction

We consider a slight modification of the cloud-shock interaction problem from Tóth [90] and Dai and Woodward [20]. In their formulation, the cloud is propagating at a constant speed toward the shock, while in our setup the bubble is initially stationary. The stationarity of the bubble makes it computationally easier to ensure that it remains in hydrostatic equilibrium with the surrounding fluid until the shock hits. The computational domain is $(x, y) \in [0, 1] \times [0, 1]$ with constant inflow conditions at the left boundary and outflow boundary conditions on the three remaining sides. The initial conditions consist of a shock located at $x = 0.05$,

$$\begin{aligned}&\Big[\rho, u_1, u_2, u_3, p, B_1, B_2, B_3\Big]_{t=0}\\ &= \begin{cases} \Big[3.86859, 11.2536, 0, 0, 167.345, 0, 2.1826182, -2.1826182\Big] & \text{if } x < 0.05 \\ \Big[1, 0, 0, 0, 1, 0, 0.56418958, 0.56418958\Big] & \text{if } x > 0.05\,, \end{cases}\end{aligned} \tag{5.73}$$

and a circular cloud of density $\rho = 10$ and radius $r = 0.15$ centered at $(x, y) = (0.25, 0.5)$. The cloud is in hydrostatic equilibrium with fluid to the right of the shock. $\gamma = 5/3$ and the initial magnetic potential is given by

$$\mathbb{A}(x, y, 0) = \begin{cases} -2.1826182x + 0.080921431 & \text{if} \quad x \le 0.05 \\ -0.56418958x & \text{if} \quad x \ge 0.05\,. \end{cases} \tag{5.74}$$

The results of a computation using the MPACT scheme on a 200×200 grid are shown in Figure 5.12. We plot contour lines of (a) the log of the density and (b) the magnetic field lines. Although our modified problem is slightly different from the setup presented in Tóth [90] and Dai and Woodward [20], we are able to demonstrate with this test problem the robustness of the MPACT scheme on a violent shock-cloud interaction.

5.6.7 Ideal MHD test: the rotor problem

The final test case which we present in this Chapter is the rotor problem considered in both [7] and [90]. The computational domain is $(x, y) \in [0, 1] \times [0, 1]$ with non-reflecting

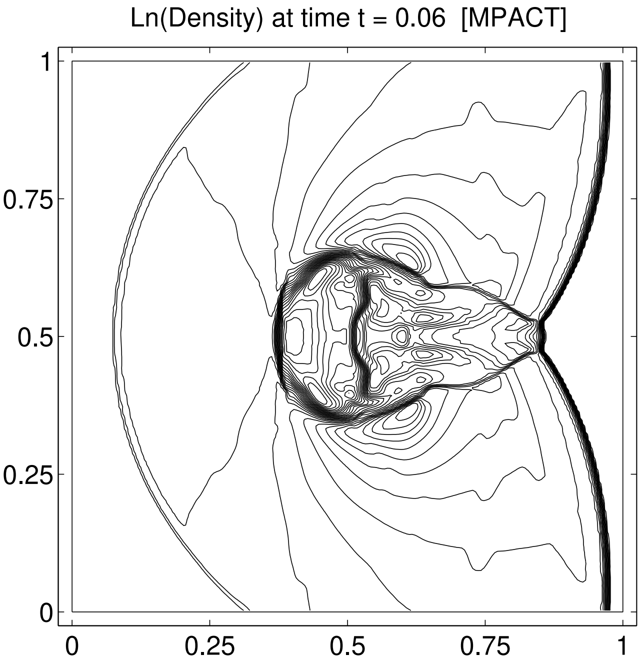

(a)

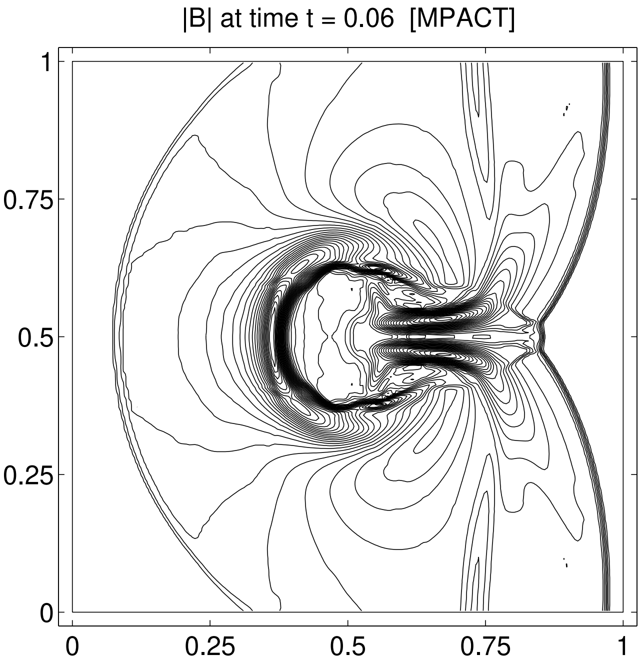

(b)

Figure 5.12: The cloud-shock interaction problem for the ideal MHD equations. Plotted are (a) the natural log of the density and (b) the magnitude of the magnetic field.

Table 5.4: Time of crash for the base scheme on three ideal MHD test problems.

TEST PROBLEM	**BASE SCHEME TIME OF CRASH***
Section 5.6.5	$t = 0.5366$
Section 5.6.6	$t = 0.0257$
Section 5.6.7	$t = 0.1627$
*Grid = 200 × 200, CFL = 0.85	

boundary conditions on all four sides. The initial conditions are given by

$$\rho(x, y, 0) = \begin{cases} 10 & \text{if} \quad r \le 0.1 \\ 1 + 9f(r) & \text{if} \quad 0.1 \le r \le 0.115 \\ 1 & \text{if} \quad r \ge 0.115 \end{cases} \tag{5.75}$$

$$u_1(x, y, 0) = \begin{cases} -(10y - 5) & \text{if} \quad r \le 0.1 \\ -(10y - 5)\, f(r) & \text{if} \quad 0.1 \le r \le 0.115 \\ 0 & \text{if} \quad r \ge 0.115 \end{cases} \tag{5.76}$$

$$u_2(x, y, 0) = \begin{cases} (10x - 5) & \text{if} \quad r \le 0.1 \\ (10x - 5)\, f(r) & \text{if} \quad 0.1 \le r \le 0.115 \\ 0 & \text{if} \quad r \ge 0.115 \end{cases} \tag{5.77}$$

$$p(x, y,) = 0.5 \tag{5.78}$$

$$B_1(x, y, 0) = \frac{2.5}{\sqrt{4\pi}} \tag{5.79}$$

$$B_2(x, y, 0) = 0 \tag{5.80}$$

$$\mathbb{A}(x, y, 0) = \left(\frac{2.5}{\sqrt{4\pi}}\right) y\,, \tag{5.81}$$

where $\gamma = 5/3$, $u_3 = B_3 = 0$, $r = \sqrt{(x - 0.5)^2 + (y - 0.5)^2}$, and $f(r) \equiv \frac{1}{3}(23 - 200r)$.

The results of a computation using the MPACT scheme on a 200×200 grid are shown in Figure 5.13. We plot contour lines of (a) the density, (b) the thermal pressure, (c) the Mach number, and (d) the magnetic pressure. These results are in good agreement with the computations of Balsara and Spicer [7] and Tóth [90].

5.6.8 The base scheme applied to ideal MHD

The three multidimensional MHD problems discussed in Sections 5.6.5, 5.6.6, and 5.6.7 have thus far only been solved using the MPACT scheme. What happens when we apply the base scheme? The answer to this question on all three test cases is simple: the base scheme always crashes. We summarize our findings in Table 5.4.

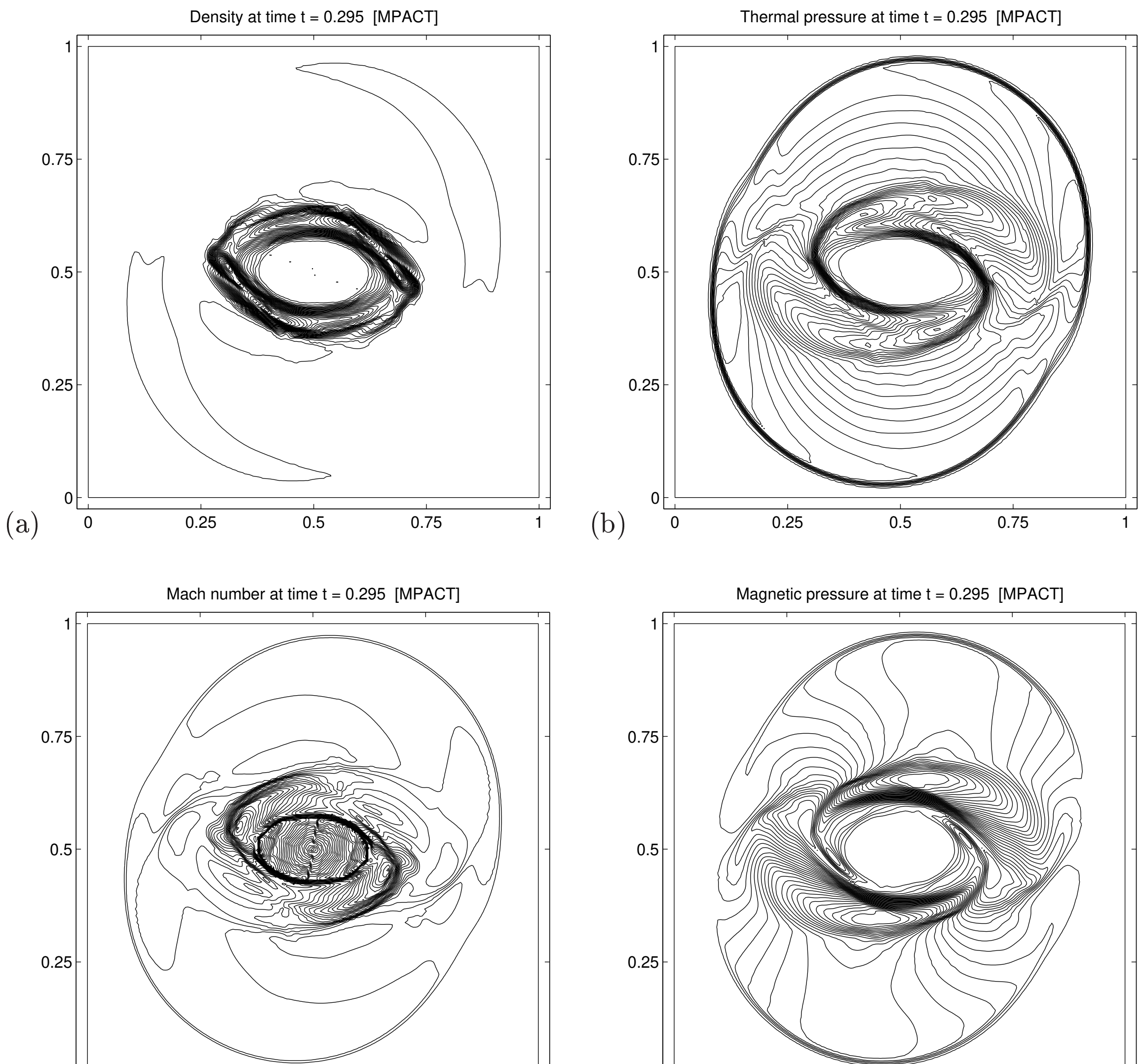

Figure 5.13: The rotor test problem for the ideal MHD equations. Plotted are (a) the density, (b) the thermal pressure, (c) the Mach number, and (d) the magnetic pressure.